A Zigzag Wall with Asymmetric Emissivity for Radiative Cooling Building Envelope

Qilong Cheng[1], Sebastian Gomez[1], Guanzhong Hu[2], Albatool Abaalkhail[1], Jazmyn E. Beasley[2], Peter Zhang[3], Yuan Xu[1], Jyotirmoy Mandal[4,5*], Aaswath P. Raman[4*], Nanfang Yu[1*], Yuan Yang[1,6*]

[1] Department of Applied Physics and Applied Mathematics, Columbia University, New York, NY 10027, USA

[2] Mechanical Engineering, Columbia University, New York, NY 10027, USA

[3] Henry M Gunn High School, Palo Alto, CA 94306, USA

[4] Department of Materials Science and Engineering, University of California, Los Angeles, Los Angeles, CA 90095, USA

[5] Department of Civil and Environmental Engineering, Princeton University, Princeton, NJ 08544, USA

[6] Lead contact

*Correspondence: yy2664@columbia.edu (Y. Yang), ny2214@columbia.edu (N. Yu), aaswath@ucla.edu (A. Raman), jm3136@princeton.edu (J. Mandal)

Abstract

Passive daytime radiative cooling (PDRC) is an attractive electricity-free approach to reducing energy consumption of buildings by reflecting sunlight and emitting infrared radiation (IR). Current PDRC research focuses on roofs, but limited attention has been paid to walls. Here, we report the control of angular asymmetry, a new degree of freedom, to realize zigzag PDRC walls with asymmetric emissivity and thus sub-ambient cooling performance. Such asymmetry leads to a daily average temperature drop of 2.3 °C compared

to conventional walls coated with PDRC materials. When the ground is at ~56 °C, the temperature drop reaches 3.1 °C, corresponding to a relative cooling power of 67 W m^{-2} compared to the control wall. The zigzag wall can provide annual total energy saving up to 37 GJ (28.2 MJ m^{-2}, ~15%), and annual total utility saving up to $1.4k (~22%) for a typical midrise apartment building, and benefit 42% population in the U.S., particularly in the southern warm areas.

Introduction

Buildings consume ~40% of global energy and account for ~36% of CO_2 emissions (*1*), and cooling constitutes ~20% of energy consumption in buildings (*2*). Therefore, efficient cooling methods are critical to reducing energy consumption and associated CO_2 emission, and expediting the transition to a carbon-neutral society. Recently, passive daytime radiative cooling (PDRC) emerged as an electricity-free approach for cooling by reflecting sunlight [wavelengths (λ) ~ 0.3 to 2.5 μm] and emitting long-wave infrared radiation (IR) through an atmospheric transparency window (ATW: λ ~ 8 to 13 μm) to the cold outer space. PDRC has drawn increasing attention in the last ten years due to advances in materials with both high solar reflectance ($R_{solar} > 0.95$) and high emittance in ATW ($\varepsilon_{ATW} > 0.95$), such as photonic structures (*3, 4*), polymers (*5-7*), metamaterials (*8, 9*), cooling wood (*10*), and composites (*11-13*). With their tailored divergent optical properties at different wavelengths (ultraviolet, visible, near-infrared, ATW), PDRC is promising to be applied to roofs (*4, 14, 15*), windows (*16, 17*), heat exchangers (*18, 19*) and greenhouses (*20*), which serve as a passive alternative to reduce energy consumption and lower carbon footprint.

While various PDRC designs have been successfully applied to rooftops that occupy limited areal portion in building envelopes, they are not ideal for walls, which cover the major portion of building envelopes. The main challenge for PDRC walls is that they face both cold space and hot ground. Thus, their radiative heat transfer with the ground needs to be taken into consideration. The ground usually has a higher surface temperature than the ambient air (dry bulb) due to the daytime solar heating and heat preservation (*21*), which can reach ~60-70 °C at the peak (*22*). Also, the ground materials (e.g., concrete, brick, asphalt) typically have high thermal emissivity $\varepsilon > 0.9$ (*23*), resulting in significant thermal radiation to the walls (e.g., ~90 W m^{-2} at 60 °C and $\varepsilon_{ground} = 0.95$). Consequently, conventional PDRC designs with a high emissivity will receive considerable heat from the ground, which are not effective for PDRC walls (Fig. 1A).

PDRC walls have gained limited attention so far, and current designs have limitations. An ATW selective emitter was reported to reflect the terrestrial thermal radiation outside of this wavelength band and keep the radiative cooling within the band (*24*), but the vertical surface still suffers strong radiation in the ATW from the ground, which accounts for ~40% of the total thermal radiation at 40-60 °C. Low-emissivity (low-E) films have been developed for building walls to reject radiation from the hot ambient environment (*25*), but the heat loss to the cold space through the ATW is also abandoned.

To break such paradox, we propose a zigzag wall structure with asymmetric emissivity, consisting of an IR emissive surface facing the sky and an IR reflective surface facing the ground [emissive/reflective zigzag (ERZ) wall], to maximize the wall's net radiative cooling power, providing a new solution to efficient thermal management of buildings. In our design (Fig. 1B), the IR emissive surface that faces the sky can still radiate the thermal emission through the ATW,

achieving PDRC. In contrast, the IR reflective surface such as metalized film faces the hot ground and reflects the infrared radiation from the ground, which decreases the heat gain.

To validate the effectiveness of this design, spectral irradiances of net heat gain from the ground and the net heat loss to the space were simulated for a conventional flat emissive wall (high-E wall, Fig. 1C) and an ERZ wall (Fig. 1D), respectively (see Supplementary Materials, Section 1). The high-E wall is assumed as an ideal broadband emitter, and the ERZ wall is composed of an ideal emitter and an ideal reflector. As shown in Fig. 1C and Fig. 1D, at a ground surface temperature of 60 °C and a wall temperature of 30 °C, the high-E wall gains 89.7 W m^{-2} from the hot ground, while the ERZ wall only receives 15.1 W m^{-2}. Such a large reduction arises from the larger view factor (0.75) from the reflective bottom surface of the ERZ wall to the ground, compared to 0.5 for the high-E wall. On the other side, the high-E wall loses 40.9 W m^{-2} heat to the space, and the ERZ wall loses a slightly higher amount of 42.2 W m^{-2}. This is due to the high view factor (0.93) of the top emissive surface to the sky in the ERZ wall, compared to 0.5 for the flat high-E wall, and the fact that the sky emittance is lower near the zenith and higher near horizon (*26*).

Consequently, the ERZ wall's effective angular emissivity is ~0.91 facing the sky, but only ~0.08 facing the ground, showing a significant angular asymmetry (Fig. 1F). In addition, an ideal low-E wall has a net heat exchange of 0 W m^{-2} because its zero emissivity does not allow any radiative heat transfer. Therefore, the ERZ wall with asymmetric emissivity can achieve more significant building cooling than flat walls with either high ε or low ε, and even sub-ambient PDRC, which is later demonstrated both numerically and experimentally.

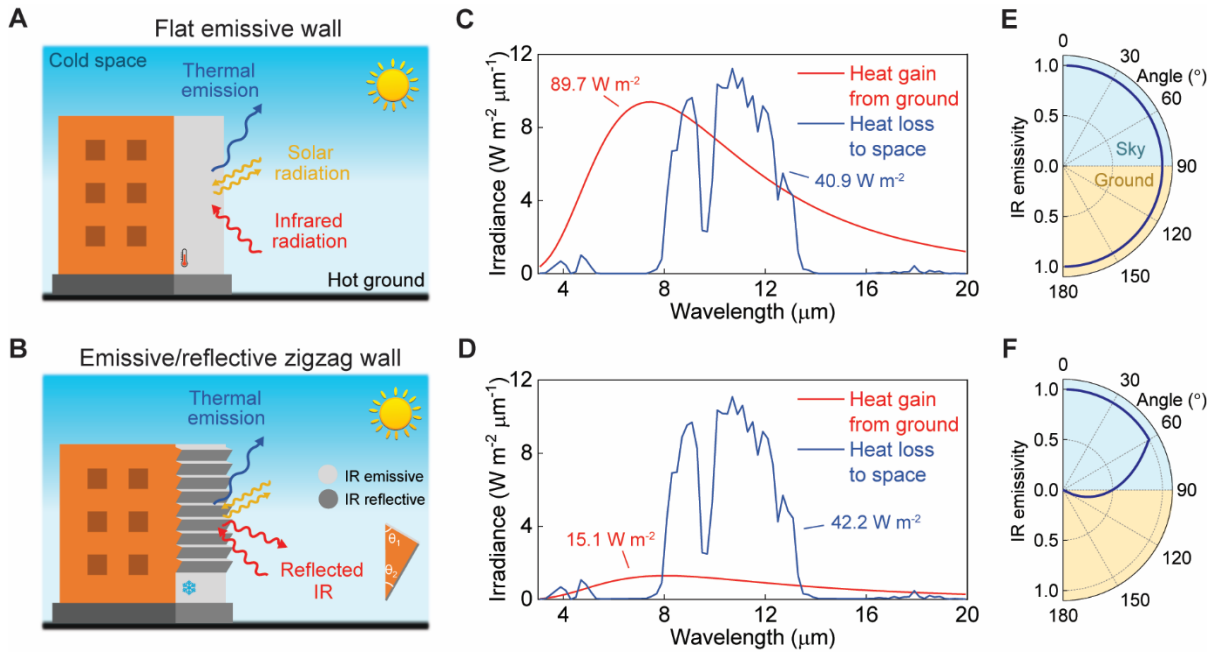

Fig. 1. Conceptual illustration of emissive/reflective zigzag (ERZ) walls. (**A**) Schematic of a conventional flat emissive wall ($\lambda \geq 2.5$ μm: $\varepsilon = 1$), showing mechanisms of its heat transfer with the surroundings. (**B**) Schematic of an emissive/reflective zigzag (ERZ) wall. Top surface: an ideal broadband emitter ($\lambda \geq 2.5$ μm: $\varepsilon_{top} = 1$). Bottom surface: an ideal broadband reflector ($\lambda \geq 2.5$ μm: $\varepsilon_{bottom} = 0$). It can reflect the IR from the hot ground while maintaining the thermal emission towards the cold space, achieving further building cooling than flat walls coated with PDRC materials. (**C-D**) Simulated net heat gain from the ground (60 °C, heat exchange between the ground and the wall) and net heat loss to the space (heat exchange between the sky and the wall) for the flat high-E wall (**C**) and the ERZ wall (**D**). The wall surfaces and the ambient are set at 30 °C. The powers are normalized by the nominal footprint wall area. The ERZ wall features a much lower heat gain (16.8%) and a slightly higher heat loss (103.2%) compared to the flat high-E wall. (**E-F**) Simulated angular IR emissivity of a flat high-E wall (**E**) and an ERZ wall (**F**). The flat high-E wall has a uniformly high emissivity facing the sky or the ground, while the ERZ wall shows a significant angular asymmetry. In (**D, F**), the ERZ wall has geometry of $\theta_1 = 60°$, $\theta_2 = 30°$.

Results

Theoretical cooling potential of ERZ walls

Unlike previous PDRC studies where the only tunable degrees of freedom are optical properties of materials, the zigzag design further utilizes a new degree of freedom, angular

asymmetry, to maximize the cooling performance. This zigzag geometry can be described by two parameters as the critical angle between the vertical direction and the top surface θ_1 or the bottom surface θ_2 (Fig. 2A). Moreover, the surface specularity also plays an important role in the cooling performance, since light can bounce between different wall surfaces for multiple times (Fig. 2B inset and Fig. 2C).

To understand the effects of the angular asymmetry and maximize the cooling performance, we first investigate the impact of specularity at (top, bottom) surfaces by calculating the relative cooling power P_{cool}, which is defined as the extra cooling power of an ERZ wall in comparison with a flat high-E wall that has the same emissivity as the side facing the sky in the ERZ wall (see Supplementary Materials, Section 1). At the (s, s) case where both the surfaces are specularly reflective, the ERZ wall shows the largest P_{cool} (Fig. 2B). Such results are also consistent with our qualitative analysis (Fig. 2C) and experimental data (Fig. S10) that specular opaque surfaces should result in less solar absorption and less IR absorption than diffuse ones, since some portion of the radiation gets reflected away without bouncing among zigzags. Similar results are also observed in other (θ_1, θ_2) combinations (Fig. S5). Therefore, both the surfaces are set at specularity of 1 in the following analysis.

The relative cooling powers P_{cool} at an extensive range of (θ_1, θ_2) combinations were further surveyed for both day (Fig. 2D) and night (Fig. 2E). In daytime, when the solar zenith angle is 30°, the relative cooling power $P_{cool} > 70$ W m^{-2} occurs at (45°-60°, 25°-35°). At night, the maximum relative cooling power P_{cool} reaches 78.6 W m^{-2} at (90°, 30°), but remains nearly a constant for (60°-90°, 25°-35°), because of almost unchanged thermal emission to the cold space and absence of solar absorption at night. At other solar zenith angles, (θ_1, θ_2) of (60°, 30°) also

achieves nearly optimal P_{cool} (Fig. S3), and their complementary values provide convenience for prototype fabrication.

The relationship between P_{cool} and varying ground surface temperatures shows that the ERZ wall provides a positive P_{cool} when the ground surface temperature exceeds ~35 °C and that a higher ground surface temperature induces a larger cooling advantage because more incoming IR is rejected (Fig. 2F). From the simulations, we also observe that the ERZ wall's cooling performance slightly deteriorates with increasing solar absorptance (Fig. S4). However, this effect is minor and can be reduced by using materials with high R_{solar} over 0.95 (Fig. S15). In addition, it should be noticed that the dimension of one zigzag period itself does not affect the cooling performance if it is significantly larger than relevant thermal wavelengths below 50 μm (Fig. S6), which guarantees convenient fabrication and scalability.

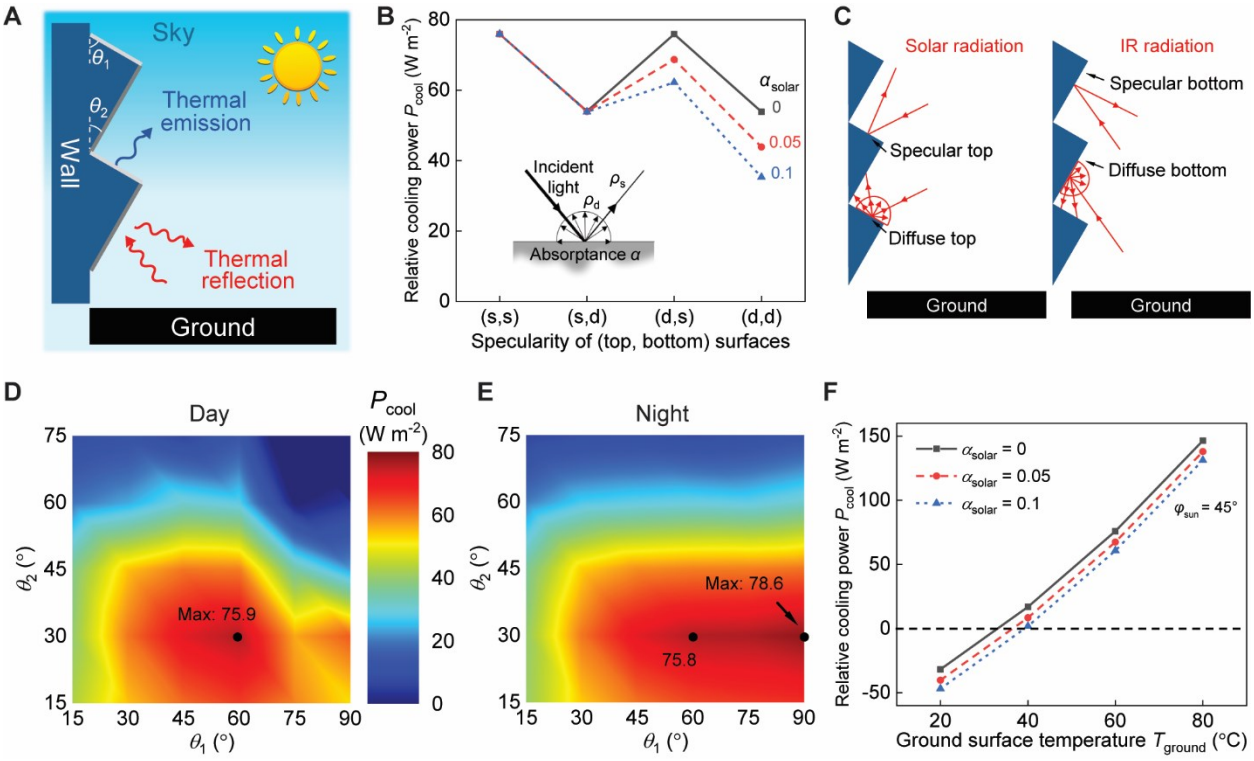

Fig. 2. Simulations on cooling performance of ERZ walls. (**A**) Schematic of the ERZ wall configuration used in the simulations, featuring two critical angles θ_1 and θ_2. (**B**) Simulated relative

cooling power P_{cool} as a function of specularity of the two surfaces (s: specularity = 1; d: specularity = 0) and their solar absorptance α_{solar}. To calculate P_{cool}, an energy flux is applied to the back of a wall to keep its exterior at the same temperature as the ambient air, and P_{cool} is the difference of the energy fluxes for the ERZ wall and the high-E wall: $P_{cool} = P_{cool,\ ERZ} - P_{cool,\ high\text{-}E}$ (Fig. S2C). Inset: schematic of diffuse reflectance ρ_d, specular reflectance ρ_s, and absorptance α for an opaque surface. Specularity is defined as $\rho_s/(\rho_s + \rho_d)$. (**C**) Schematics showing how specularity reduces solar absorption and IR absorption among zigzags. (**D-E**) P_{cool} contours over θ_1 and θ_2 with sunlight present (**D**) or without sunlight (**E**). The solar absorptance α_{solar} is set as 0.05 on all wall surfaces. (θ_1, θ_2) = (60°, 30°) leads to optimal results. (**F**) The relationship between P_{cool} and the ground surface temperature. In (**B, D**), the solar zenith angle is 30° to represent a typical case for afternoons in the southern U.S., while the solar zenith angle is 45° in (**F**) to show the effect of enhanced solar absorption on the wall from light bouncing. P_{cool} contours at other solar zenith angles of 0°, 60°, 90° are presented in Fig. S3. In (**B, D, E**), the ground surface temperature is always 60 °C.

Cooling performance of ERZ walls

To experimentally demonstrate the cooling performance of ERZ walls, we fabricated samples with scalable and low-cost materials as a proof of concept. Aluminized Mylar films were used as the IR reflector facing the hot ground since they have a specularity > 0.98 (Fig. 3A). Polydimethylsiloxane (PDMS, ~150 μm) coated Mylar films were used as the IR emitter that faces the sky due to high thermal emissivity and optical transparency of PDMS (*27*), which retains a high specularity ~0.94 (Fig. 3B). The reflector and the emitter show nearly identical solar reflectance (~0.87), while their IR emittances (0.08 and 0.94) differ greatly.

The reflectors and the emitters were attached on aluminum parts, which were laminated on substrate with its back affixed with a thermocouple (TC) and sealed with polystyrene (PS) foam as heat insulation (Fig. 3C and Fig. 3D). The hollow of the aluminum parts at the sample lateral surfaces was covered with aluminum tape. The thermocouple was positioned at the center of the substrate back surface to capture the average temperature of the sample. As the zigzag feature size

is in the scale of centimeter, it is convenient to fabricate such structures by molding in a scalable fashion.

Significant cooling was observed in the ERZ wall prototype compared to each of (a) a flat wall covered only with PDMS/Al/Mylar emitters (high-E wall), (b) a flat wall covered only with Al/Mylar reflectors (low-E wall), and (c) a wall with the same zigzag structure but only PDMS/Al/Mylar emitters [emissive/emissive zigzag (EEZ) wall]. First, in lab tests with a simulated sky made of ice/water mixture and a ground made of cinefoil heated to 60 °C (Fig. S8), the ERZ wall's temperature rise is 2.9, 1.6, and 2.8 °C lower than that of the high-E wall, the low-E wall, and the EEZ wall, respectively, under simulated day condition (Fig. 3E). During night, the ERZ wall is 3.0, 1.3, and 2.8 °C cooler than the three controls, respectively. The experimental results also show that the optimal cooling performance is achieved at $\theta_1 = 60°$ under the constraint of $\theta_1 + \theta_2 = 90°$, which agrees well with the simulation results (Fig. 3F and Fig. 2D). It should be noted that the simulated ice/water sky is not as cold as the real sky, and it has a limited view factor for the wall samples, so the radiative cooling to the simulated sky in the lab tests is not as efficient as the real sky. Thus, the lab tests show temperature rise instead of temperature drop as compared to the ambient temperature.

Following the success in the lab tests, we further demonstrate the advantages of ERZ walls in field tests, which were carried out in summer 2022 in New Jersey, USA (Fig. 3G and Fig. S12). As shown in Fig. 3H, the ERZ wall was always cooler than the control (high-E wall) for a continuous 24 hours, where the ground surface temperature ranged from 23 °C (07:06) to 56 °C (14:29). The ERZ wall was also cooler than the ambient air temperature in most time (20:00-10:47 and 16:35-20:00) except the hottest period (10:47-16:35) when the ground (> 45 °C) gave off the strongest thermal radiation, which was absorbed by the top emissive surface after specular

reflection at the bottom surface. Nevertheless, the average temperature of the ERZ wall was still 1.2 °C lower than the ambient air. Also, another field test shows that the ERZ wall was averagely 1.0 °C cooler than the low-E wall (Fig. S13), demonstrating the advantage of the ERZ wall. The temperature simulation shows consistent results, and further confirms that the ERZ wall performs better than the wall with a single valued emissivity, no matter high-E or low-E (Fig. S14A).

In comparison with the high-E control, the temperature of the ERZ wall was 2.3 °C lower on average, and this value reached a peak of 3.1 °C between 13:00 and 14:00 (Fig. 3I). This appears counterintuitive since it indicates that the most pronounced cooling occurred at the hottest time. Such a phenomenon can be explained as that the calculated temperature difference is between the ERZ wall and the flat high-E wall, instead of between the ERZ wall and the ambient, so the high ground surface temperature at 13:00-14:00 (> 50 °C) enlarges the difference of heat absorption at these two walls from the ground, leading to the maximum temperature difference between them. The temperature drop also shows a good agreement with the simulation (Fig. 3I).

We further estimate the relative cooling power P_{cool} of the ERZ wall from the temperature data in Fig. 3H, which is in the range of 30 to 67 W m^{-2} in a day (Fig. 3J, see Supplementary Materials, Section 3). Similarly, the P_{cool} shows the same trend as the temperature drop that its peak 67 W m^{-2} appeared at the hottest period of 12:00-15:00, which also coincides with the data in Fig. 1C and Fig. 1D (heat rejection ~76 W m^{-2}). In addition to the experiments above, we also tested the ERZ wall facing southwest, and the temperature drop reached ~2.6 °C (Fig. S16), demonstrating that the cooling effect is generic. Moreover, we tested the ERZ walls partially covered by polyethylene films, which further reduces heat exchange due to air convection but still allows infrared radiation to pass. A larger temperature drop of ~4.7 °C compared to the high-E wall was achieved (Fig. S17), indicating further potential to enhance the cooling performance.

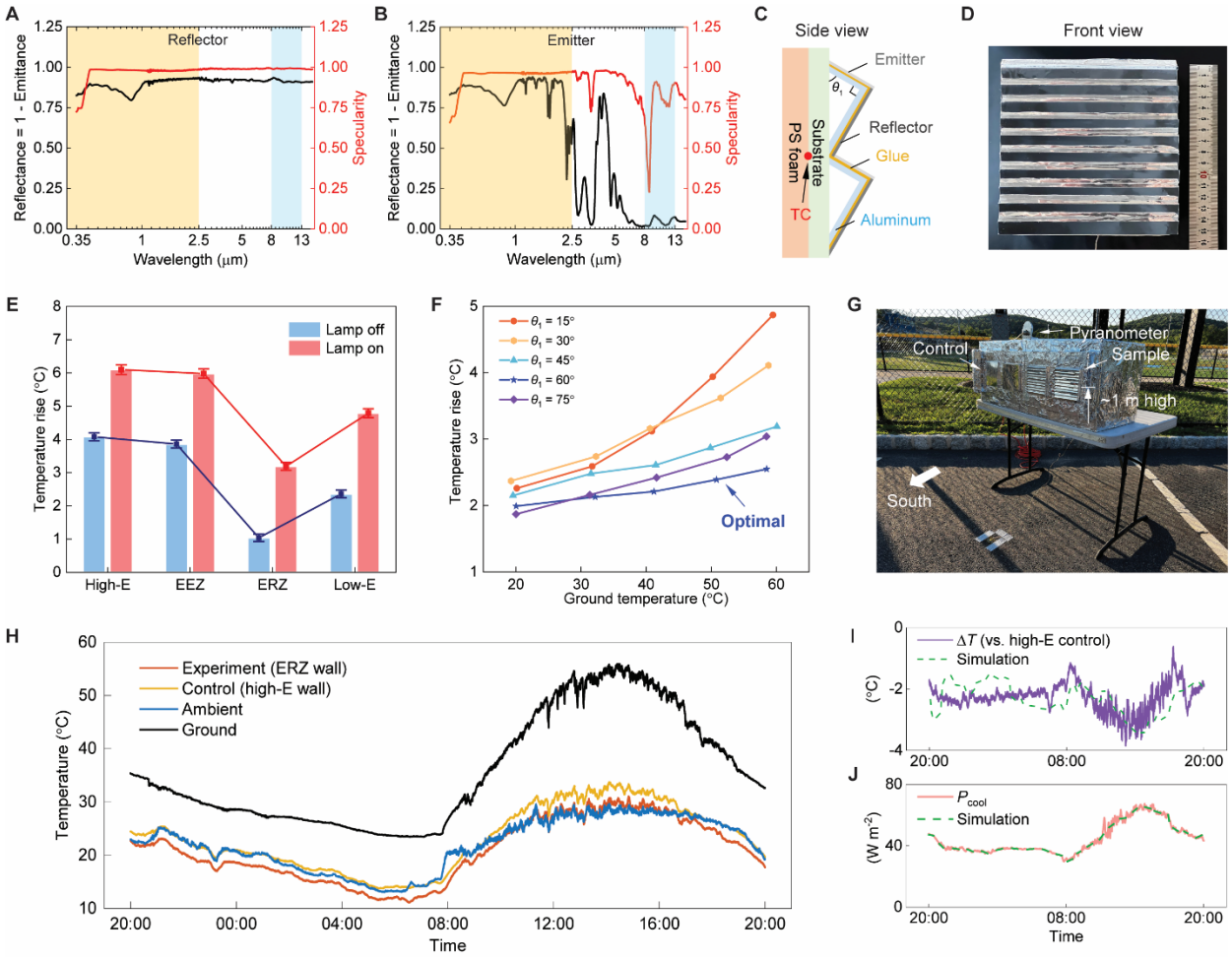

Fig. 3. Fabrication of ERZ walls and experiments on its cooling performance. (**A-B**) Spectral reflectance [$\rho(\lambda) = 1 - \varepsilon(\lambda)$] and specularity of the reflector (**A**) and the emitter (**B**) which covers the ERZ wall. They have nearly the same reflectance in the solar spectrum (0.87 for A vs. 0.86 for B) and high specularities in the whole spectrum. (**C**) Schematic of the ERZ wall fabrication. The critical angles θ_1 and θ_2 are complementary for simplicity of fabrication. (**D**) Front view of the ERZ wall sample. The sample is 15 cm × 15 cm. (**E**) Steady average temperature data of various samples in lab tests ($\theta_1 = \theta_2 = 45°$). The lamp irradiance on the samples is ~81 W m^{-2}. (**F**) The dependence of temperature rise on θ_1 at different ground surface temperatures for the ERZ wall. Error bars are < 0.15 °C. (**G**) The experimental setup for field tests in Sparta Township, NJ. (**H**) Temperature data over a continuous 24 hours. The solar irradiance peaked at ~460 W m^{-2} facing south or ~930 W m^{-2} facing upward (Fig. S12C). (**I-J**) Temperature drop ΔT (**I**) and relative cooling power P_{cool} (**J**) of the ERZ wall as compared to the high-E control.

Besides results based on the low-cost PDMS/Al/Mylar surfaces, full-day sub-ambient cooling is achieved by using a silver-coated ERZ wall with a higher R_{solar} of 0.95 (Fig. 4A and Fig. S15). In the continuous 24 hours, the silver ERZ wall was cooler than the high-E control by 2.2 °C on average (Fig. 4B), and the temperature drop reached 3.2 °C at 14:00-15:00. The silver ERZ wall was also always cooler than the ambient air by 1.4 °C on average, and their difference maximized at -6 °C at the first sunshine (Fig. 4C). In the hot afternoon (12:00-17:00), the silver ERZ wall was still 0.26-1.29 °C cooler than the ambient temperature. The experimental data are consistent with the simulation results (Fig. S15C). Moreover, the simulation again shows that the ERZ wall outperforms the low-E wall.

Discussion

Effects of thermal insulation

In the aforementioned experimental validation, we used thin polyacrylate walls with a low thermal resistance ($R = 8.0\times10^{-3}$ m^2 K W^{-1}) to align with previous experiments on cooling roofs (*4-6, 10*). For practical thicker walls, the simulation results (Fig. S14B) show that up to the standard thermal insulation (2 m^2 K W^{-1}), there is no significant change in the average $T_{ERZ,\ interior} - T_{high\text{-}E,\ interior}$ (e.g., -2.3 °C for R from 8.0×10^{-3} m^2 K W^{-1} to 1 m^2 K W^{-1} and -2.2 °C for 2 m^2 K W^{-1}). Here, $T_{ERZ,\ interior}$ and $T_{high\text{-}E,\ interior}$ are defined as the temperature at the back of the thermal insulation layer, which corresponds to indoor wall temperature (Fig. S14A inset). When R further increases to 5 m^2 K W^{-1}, the variations in $T_{ERZ,\ interior} - T_{high\text{-}E,\ interior}$ are delayed, and the average of $T_{ERZ,\ interior} - T_{high\text{-}E,\ interior}$ remains at -1.3 °C for 5 m^2 K W^{-1}, which is still remarkable.

Energy savings of ERZ walls

To quantify the potential energy savings of ERZ walls at different climate zones, we conducted simulations of energy consumption in buildings using EnergyPlus (see Supplementary Materials, Section 4). In the simulations, a midrise apartment building with ERZ walls on all four sides was compared with the same building with flat high-E walls (Fig. 4D). The building is a commercial reference defined by the US Department of Energy (DOE) (*28*). Standard thermal insulation provided by the DOE reference was applied in all simulations. The only input used in the EnergyPlus simulations is the spectra properties of the emissive surface (R_{solar} = 0.95, $\varepsilon_{thermal}$ = 0.95) and the reflective surface (R_{solar} = 0.95, $\varepsilon_{thermal}$ = 0.05), but not near-surface temperature measured in Fig. 3H.

In the summer, the ERZ wall can provide annual cooling energy saving of 10-34 GJ or 7.6-26.0 MJ m^{-2} (2-29%) as compared to the high-E wall for a midrise building in 11 cities in the U.S. and 3 international cities (Fig. 4E and Fig. 4F). Particularly, Los Angeles, San Francisco, and Cape Town show the largest cooling gain of ~30 GJ (22.9 MJ m^{-2}), indicating that the ERZ design is best for warm weather. Similarly, the annual saving map of cooling energy shows that the cooling gain changes from ~34 GJ (26.0 MJ m^{-2}) in the southwest down to ~10 GJ (7.6 MJ m^{-2}) in the north (Fig. 4G).

To comprehensively understand the energy impact of ERZ walls, the heating penalty in winter should also be taken into account. For the year-round savings, we chose 16 representative cities respectively in the 16 climate zones in the U.S. (*29*), and mapped the annual energy savings and utility savings in the U.S. (Fig. 4H and Fig. S21). The maps demonstrate that for a midrise apartment building, the ERZ wall can provide annual total energy saving up to 37 GJ (28.2 MJ m^{-2}, Fig. S21C) and ~15% (Fig. S21D), which corresponds to annual total utility saving up to $1.4k

(Fig. S21E) and ~22% (Fig. 4H/Fig. S21F) in most of the southern U.S. This area where the ERZ wall has net savings accounts for 27% of the land area and 42% of the population (Fig. 4H). In these regions, warm summers and mild winters make the cooling utility saving outweigh the heating penalty. In cold regions, the benefit in cooling is overshadowed by the increased heating demand. Moreover, the ERZ wall can still reach attractive cooling performance and energy saving when it is surrounded by adjacent buildings, such as an annual total energy saving of 29.5 GJ (22.5 MJ m^{-2}) in Los Angeles at a building-to-building distance of 10 m (Fig. S22). Meanwhile, for buildings with different volume-to-wall-surface ratios (e.g., larger buildings), the ERZ wall still provides effective savings > 22 MJ m^{-2} and > 9% compared to the conventional high-E wall (Fig. S23).

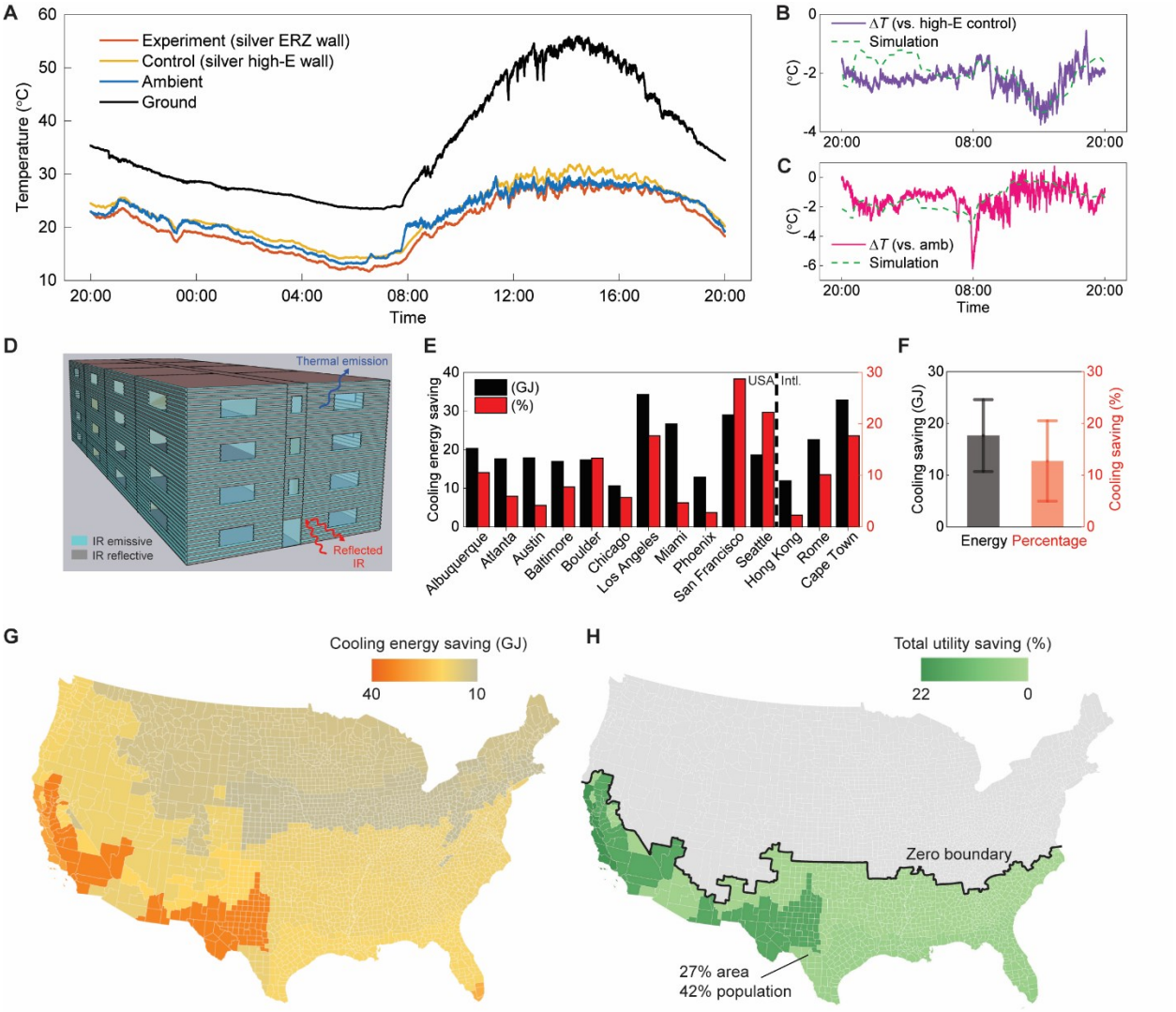

Fig. 4. Sub-ambient cooling performance and potential energy savings of ERZ walls. (**A**) Temperature data of silver ERZ wall over a continuous 24 hours. The samples were measured at the same time as Fig. 3H. (**B**) Time-dependent temperature drop ΔT between the silver ERZ wall and the silver high-E control. (**C**) Time-dependent temperature drop between the silver ERZ wall and the ambient temperature. (**D**) The midrise apartment building model used in EnergyPlus simulations, with ERZ walls. (**E**) Annual cooling energy saving and percentage of a midrise building with ERZ walls as compared to the same building with high-E walls among 11 cities in the U.S. and 3 international cities. (**F**) Average annual cooling saving and percentage of the 11 cities in the U.S. together with their standard deviations. (**G-H**) Annual saving maps of cooling energy (**G**) and total utility (**H**) of a midrise building with ERZ walls as compared to the same building with high-E walls.

Reducing light pollution and scalable manufacturing

The optimized ERZ walls consist of emitters and reflectors with high specularity. One potential issue of such high specularity is light pollution, but this can be addressed by using a thin layer of visibly opaque but IR transparent nanoporous polyethylene (nano-PE) as the cover. The diffuse reflection of nano-PE in visible light renders a diffuse appearance, but its high IR specular transmittance > ~80% in 8-13 μm at incident angles of 0-70° indicates that it does not affect the radiative heat transfer between the ERZ walls and the surroundings (Fig. S11). Also, the scalable production of nano-PE makes it suitable for such a large-area application in the building envelopes (see Supplementary Materials, Section 2). On the other side, it should be noted that nano-PE and PE films are not widely used as building materials. Their limitations and challenges need to be further evaluated for practical applications.

The zigzag walls could also be manufactured in a large scale. First, using a larger period of zigzag repeating unit of 5-50 cm instead of ~1.5 cm in the paper does not compromise optical performance since the geometric dimension is much larger than wavelengths of interest. Such larger structures can be manufactured by using a mold to press metal sheet first, followed by applying high-E coating (e.g., applying a paint or laminating a film) to the side facing the sky, and applying low-E coating (e.g., laminating a reflective film) to the side facing the ground. Moreover, the wide use of wave-like corrugated walls with cm-scale corrugation in building envelopes further validates the feasibility of large-scale manufacturing of the zigzag walls (*30*).

Conclusion

We developed a zigzag wall structure with asymmetric emissivity for reducing energy consumption in buildings. The ERZ wall exhibits superior cooling than conventional walls with

either high emissivity or low emissivity, since it can simultaneously reflect the thermal radiation from the hot ground and remain emissive to the cold space. The cooling performance was confirmed by steady-state simulations, real-world field tests, and EnergyPlus simulations. Such structures can also be fabricated in a scalable fashion by simple molding. Furthermore, the ERZ wall can also be combined with state-of-the-art daytime PDRC materials or responsive PDRC materials to further enhance the thermal efficiency of building envelopes. Such diverse possibilities make the ERZ wall a viable pathway for smart and sustainable buildings.

Acknowledgements

We thank Sparta High School for providing the site to carry out the field tests. YY acknowledges support from the National Science Foundation (Award No. 2005747) and Urban Tech Award. JM acknowledges support from Schmidt Science Fellows, in partnership with the Rhodes Trust, and Princeton University faculty startup fund.

References

1. U.S. Energy Information Administration, (2022). *Monthly Energy Review: October 2022*. Retrieved from https://www.eia.gov/totalenergy/data/monthly/previous.php.
2. International Energy Agency, (2018). *The Future of Cooling*. Retrieved from: https://www.iea.org/reports/the-future-of-cooling.
3. E. Rephaeli, A. Raman, S. Fan, Ultrabroadband Photonic Structures To Achieve High-Performance Daytime Radiative Cooling. *Nano Letters* **13**, 1457-1461 (2013).
4. A. P. Raman, M. A. Anoma, L. Zhu, E. Rephaeli, S. Fan, Passive radiative cooling below ambient air temperature under direct sunlight. *Nature* **515**, 540-544 (2014).
5. J. Mandal *et al.*, Hierarchically porous polymer coatings for highly efficient passive daytime radiative cooling. *Science* **362**, 315-319 (2018).
6. D. Li *et al.*, Scalable and hierarchically designed polymer film as a selective thermal emitter for high-performance all-day radiative cooling. *Nature Nanotechnology* **16**, 153-158 (2020).
7. J. Li *et al.*, Protecting ice from melting under sunlight via radiative cooling. *Science Advances* **8**, (2022).
8. M. M. Hossain, B. Jia, M. Gu, A Metamaterial Emitter for Highly Efficient Radiative Cooling. *Advanced Optical Materials* **3**, 1047-1051 (2015).
9. Y. Zhai *et al.*, Scalable-manufactured randomized glass-polymer hybrid metamaterial for daytime radiative cooling. *Science* **355**, 1062-1066 (2017).
10. T. Li *et al.*, A radiative cooling structural material. *Science* **364**, 760-763 (2019).

11. Y. Tian *et al.*, Superhydrophobic and Recyclable Cellulose-Fiber-Based Composites for High-Efficiency Passive Radiative Cooling. *ACS Applied Materials & Interfaces* **13**, 22521-22530 (2021).

12. K. Zhou *et al.*, Three-Dimensional Printable Nanoporous Polymer Matrix Composites for Daytime Radiative Cooling. *Nano Letters* **21**, 1493-1499 (2021).

13. P. Yao *et al.*, Spider‐Silk‐Inspired Nanocomposite Polymers for Durable Daytime Radiative Cooling. *Advanced Materials*, (2022).

14. K. Tang *et al.*, Temperature-adaptive radiative coating for all-season household thermal regulation. *Science* **374**, 1504-1509 (2021).

15. R. Levinson *et al.*, Methods of creating solar-reflective nonwhite surfaces and their application to residential roofing materials. *Solar Energy Materials and Solar Cells* **91**, 304-314 (2007).

16. S. Wang *et al.*, Thermochromic smart windows with highly regulated radiative cooling and solar transmission. *Nano Energy* **89**, (2021).

17. S. Wang *et al.*, Scalable thermochromic smart windows with passive radiative cooling regulation. *Science* **374**, 1501-1504 (2021).

18. E. A. Goldstein, A. P. Raman, S. Fan, Sub-ambient non-evaporative fluid cooling with the sky. *Nature Energy* **2**, (2017).

19. D. Zhao *et al.*, Subambient Cooling of Water: Toward Real-World Applications of Daytime Radiative Cooling. *Joule* **3**, 111-123 (2019).

20. H. Zou *et al.*, Eliminating greenhouse heat stress with transparent radiative cooling film. *Cell Reports Physical Science*, (2023).

21. B. Kallas, Asphalt pavement temperatures. *Highway Research Record*, (1966).

22. A. Mohajerani, J. Bakaric, T. Jeffrey-Bailey, The urban heat island effect, its causes, and mitigation, with reference to the thermal properties of asphalt concrete. *Journal of Environmental Management* **197**, 522-538 (2017).

23. R. Albatici, F. Passerini, A. M. Tonelli, S. Gialanella, Assessment of the thermal emissivity value of building materials using an infrared thermovision technique emissometer. *Energy and Buildings* **66**, 33-40 (2013).

24. J. Mandal, S. Mandal, J. Brewer, A. Ramachandran, A. Pattabhi Raman, https://arxiv.org/abs/2006.11931. 2020.

25. Y. C. Peng *et al.*, Coloured low-emissivity films for building envelopes for year-round energy savings. *Nature Sustainability* **5**, 339-347 (2022).

26. C. G. Granqvist, A. Hjortsberg, Radiative cooling to low temperatures: General considerations and application to selectively emitting SiO films. *Journal of Applied Physics* **52**, 4205-4220 (1981).

27. L. Zhou *et al.*, A polydimethylsiloxane-coated metal structure for all-day radiative cooling. *Nature Sustainability* **2**, 718-724 (2019).

28. M. Deru *et al.*, US Department of Energy commercial reference building models of the national building stock. (2011).

29. International Energy Conservation Code, (2012). *IECC Climate Zone Map*. Retrieved from https://basc.pnnl.gov/images/iecc-climate-zone-map.

30. Corrugated Steel Sheets Market: Global Industry Analysis and Forecast (2023-2029). Retrieved from https://www.maximizemarketresearch.com/market-report/global-corrugated-steel-sheets-market/100759/. (2023).

31. Spectral Sciences, Inc. *MODTRAN*. Retrieved from http://modtran.spectral.com/modtran_home.

32. Z. J. D. o. s. t. p. p. Wang, Chapter 2-The Solar Resource and Meteorological Parameters. 47-115 (2019).

33. https://www.gminsights.com/industry-analysis/battery-separator-market. (2021).

34. A. Hagishima, J. J. B. Tanimoto, Environment, Field measurements for estimating the convective heat transfer coefficient at building surfaces. **38**, 873-881 (2003).

35. T. Hoyt, E. Arens, H. Zhang, Extending air temperature setpoints: Simulated energy savings and design considerations for new and retrofit buildings. *Building and Environment* **88**, 89-96 (2015).

36. EnergyPlus 22.1. *Engineering Reference*. Retrieved from https://bigladdersoftware.com/epx/docs/22-1/engineering-reference/outside-surface-heat-balance.html#outside-surface-heat-balance.